aerospace

MDPI

Article

Prepositive Synergistic Bulge Design for Improving Aerodynamic Performance of Submerged Inlet

Xuan Bai and Baigang Mi *

School of Aeronautics, Northwestern Polytechnical University, Xi'an 710072, China; baixuan@mail.nwpu.edu.cn
* Correspondence: mibaigang@163.com

Abstract: A submerged inlet has good stealth characteristics and a low external drag, but it also has the disadvantage of low internal flow efficiency. In view of this, a new efficiency enhancement method based on the prepositive synergistic bulge of the inlet's anterior lip is proposed. Taking the submerged inlet of an aircraft as the baseline configuration, a miniature bulge with a square bottom and an outer convex form is designed in front of the inlet's anterior lip. Through the convex shape of the bulge, part of the low-energy boundary layer airflow is diverted away from the inlet's entrance, so that the airflow greatly reduces the flow separation after entering the inlet, and the internal flow performance of the entire submerged inlet is improved. Taking the flow field of an aircraft in the classic cruise state as an example, the simulation analysis results show that the flow field characteristics of the entire submerged inlet are obviously improved after adding the synergistic bulge. The total pressure recovery coefficient of the new inlet configuration increased by 1.36%, the total pressure distortion index decreased by 10.86%, and the body drag only increased by 0.37% compared with the baseline case. According to calculations of synergistic bulge inlet configurations with different design parameters, the effect of this configuration is relatively stable, whereby the aspect ratio of the bulge has the greatest impact on the performance, and its value should not be less than 0.75. In addition to the advantages of not requiring additional components or occupying space and being easy to manufacture, the method of adding a synergistic bulge can improve the aerodynamic performance of the baseline inlet under most cruise flight conditions, and its additional drag is small, which gives it a wide applicability range.

Keywords: submerged inlet; computational fluid dynamics (CFD); synergistic bulge; total pressure recovery coefficient; boundary layer

Citation: Bai, X.; Mi, B. Prepositive Synergistic Bulge Design for Improving Aerodynamic Performance of Submerged Inlet. *Aerospace* **2023**, *10*, 649. https://doi.org/10.3390/aerospace10070649

Academic Editor: Sergey Leonov

Received: 18 June 2023
Revised: 16 July 2023
Accepted: 18 July 2023
Published: 20 July 2023

1. Introduction

Modern air combat not only requires the aircraft to have high tactical and technical performance, but also requires improving its own survivability. The stealth performance of aircraft is particularly important in the future over-the-horizon warfare [1]. Compared with traditional inlets, the integrated design features of submerged inlets and aircraft fuselage have many advantages. In addition to effectively reducing the radar scattered area and improving the survivability of aircraft, this kind of inlet can also greatly reduce the windward area and drag of the aircraft, and is conducive to the placement of aircraft, carrying, and box launch [2–4]. However, a submerged inlet is directly open to the fuselage surface. At the small angles of attack it is impossible to make full use of the incoming high-energy flow to stamp the intake air, resulting in difficult intake of the inlet. In addition, the submerged inlet will inhale a large amount of low-energy boundary layer of airframe during the intake process, and the internal flow field is prone to generate a separation vortex, which reduces the total pressure recovery coefficient of the inlet, increases the distortion, and seriously hinders the application of submerged inlets in practical engineering. Therefore, how to improve aerodynamic performance of submerged inlets has become a key issue. Many scholars have conducted series of research on it, including the optimization of the

design of the inlet shape [5–9], the application of active flow control methods such as jet [10–16], and the exploration of passive flow control methods such as setting synergistic components near the inlet [17–27].

Among them, the active and passive flow control methods are usually redesigned on the optimized inlet configuration. But the active flow control method requires additional actuators such as gas path, controller, and power supply, and sometimes requires large energy input. So, the passive flow control method has stronger engineering applicability. Taskinoglu et al. [17–20] improved the exit flow field by installing a large-scale vertical wing spoiler in the submerged inlet's inner channel, and optimized the geometric and position parameters of the spoiler using three-dimensional numerical simulation. Furthermore, the performance of the baseline inlet and the optimized inlet was compared in the experimental study. They found that this method can greatly reduce the total pressure distortion, but that the total pressure recovery coefficient is not significantly improved. Pérez et al. [21] numerically simulated and analyzed the conventional NACA submerged inlet's flow characteristics, and delta wing vortex generators were set up to reduce boundary layer thickness. Compared with the baseline inlet, the mass flow rate of the submerged inlet with delta wing vortex generators is increased by about 20%, but 10% of the total drag comes from the vortex generators. Cheng et al. [22] set up a pair of bleeding vent slots on the side wall of the submerged inlet's inner channel, whose exits lead to the outer surface of the projectile, thus forming two channels capable of bleeding vortex and low-energy airflow. The computed results show that the total pressure recovery coefficient is increased by 2.8% and the distortion index is decreased by 51.0% compared with the baseline inlet under the design condition. When adopting this configuration, the inlet's design position on the aircraft should be taken into special consideration, and the position of the bleeding vent slots has great effect on the performance of the inlet. Sun et al. [23] used a unique bump-shaped vortex generator on the projectile's upstream surface, and verified this method using wind tunnel tests. The vortex generator improves the entrance flow quality of the inlet and then improves the submerged inlet's performance by eliminating the low-energy flow of the upstream forebody boundary layer. Saheby et al. [24] designed a submerged inlet with a triangular entrance, and they used numerical simulation method to study the influence of the ridge structure on the aerodynamic efficiency of the inlet. The results show that the ridge structure can split the boundary layer before the inlet's entrance, but it is necessary to ensure that the swirling vortex of the side edge of the inlet can pass through safely. Xie et al. [25] proposed a method to remove part of the low-energy boundary flow and improve the inlet's performance by setting a submerged deflector in front of submerged inlet and studied it through numerical simulation and wind tunnel tests. After adding the submerged deflector, the inlet's total pressure recovery coefficient is increased by 3.3%, and its circumferential distortion DC60 is reduced by 28.2%. In addition, they also studied and calculated a flow control method combining the drainage channel and the vortex roll structure [26]. This method increases the inlet's total pressure recovery coefficient by 3.06% and decreases its DC60 by 72.57%. However, the deflector and the drainage channel themselves occupy a large space, which results in higher design requirements for the aircraft configuration. Askari et al. [27] studied the effect of a bump on the performance of a Y-shaped diverterless supersonic inlet in detail using experimental and numerical methods. The results show that the existence of a bump designed in coordination with the cowl lip helps the DSI to remove the boundary layer from the inlet without adding any auxiliary systems or moving parts. This research is aimed at the supersonic case: whether this method of adding a bump before the inlet's entrance can be used in the subsonic submerged inlet needs further research. In addition, the inlet is susceptible to high flow instability and distortion, and the secondary flow and the separation of local flow will cause the AIP surface of the inlet to show complex total pressure and a swirl distortion field [28–30]. Therefore, while using the new configuration to improve the performance of the inlet, the change in swirl distortion and unsteady characteristics of the inlet's exit are also areas to which attention needs to be paid.

Based on the above research, this paper proposes a method to increase the inlet's efficiency by adding a prepositive synergistic bulge on the airframe before the inlet's entrance. Firstly, the internal flow characteristics of the baseline inlet are analyzed to explore the influencing factors of reducing the submerged inlet's aerodynamic performance. Then, a prepositive synergistic bulge inlet configuration is designed and calculated, and the mechanism of its performance improvement and the influence of the change in design parameters on the inlet's aerodynamic performance are studied. Moreover, the aerodynamic characteristics of synergistic bulge inlet configurations and the baseline inlet under different flight conditions are compared to verify the feasibility and applicability of the configuration on the consideration of the influence of the internal flow and external flow. The prepositive synergistic bulge has the advantages of small size and simple configuration, and can be added without changing the original layout of the aircraft. The design of this bulge is similar to the bump in front of the DSI inlet, so it has relatively mature application experience and engineering manufacturing methods, which makes it easy to use.

2. Baseline Model and Numerical Method Validation

2.1. Baseline Model of Submerged Inlet

Figure 1 shows the baseline submerged inlet configuration of the main intake system of an aircraft. The inlet is located on the projectile's lower abdomen plane and it adopts a trapezoidal cross-sectional shape with an inlet side angle of 4°. The outlet diameter of the inlet is d = 65 mm and the total length is 4.1 d; the distance between the most forward point of the aircraft and the leading edge of the inlet is 12 d and the distance between the exit center and the abdomen plane of the projectile is 0.88 d. The variation law of the inlet's centerline and the distribution law of the centerline along the area are consistent with reference [5].

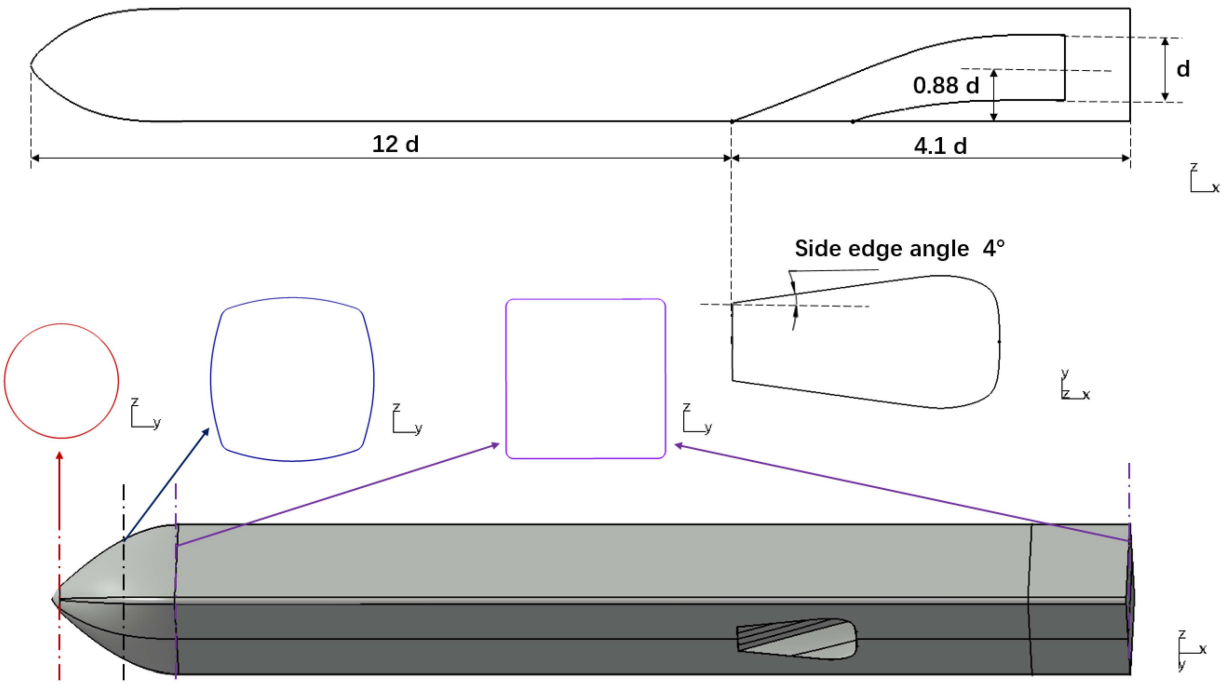

(**a**)

Figure 1. *Cont.*

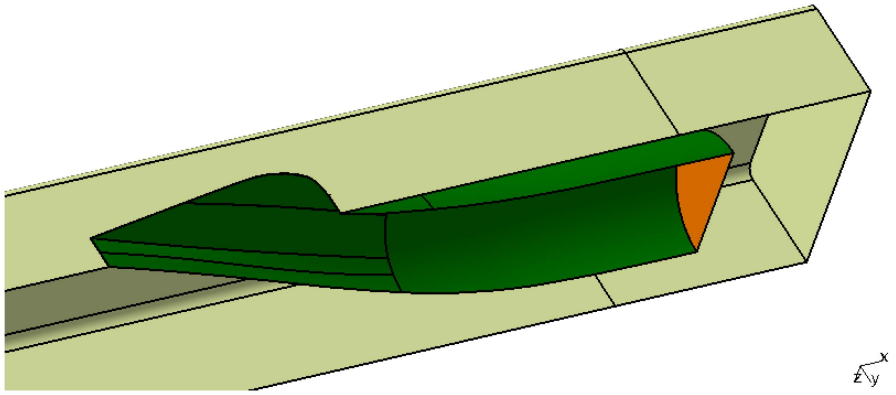

(**b**)

Figure 1. Baseline configuration of a submerged inlet. (**a**) A 3D view and sections of projectile and inlet. (**b**) Submerged inlet.

2.2. Numerical Calculation Method and Grid Division

This paper used FLUENT software for three-dimensional numerical simulation, adopted the Navicr–Stokes (N-S) equation solver based on a finite volume method, and used a shear stress ($k-\omega$SST) turbulence model [31] for calculation. An unstructured polyhedral mesh is used to mesh the submerged inlet model. And the far field is a cuboid with a length of 40 m, a width of 10 m, and a height of 10 m, as shown in Figure 2. The far field of the calculation domain adopts the pressure-far-field boundary, the projectile and inlet adopt the non-slip wall boundary, and the boundary layer is set on the object's surface. The back pressure is given to ensure the average Mach number M_e on the inlet's exit section, so that the pressure outlet boundary is adopted at the inlet's exit.

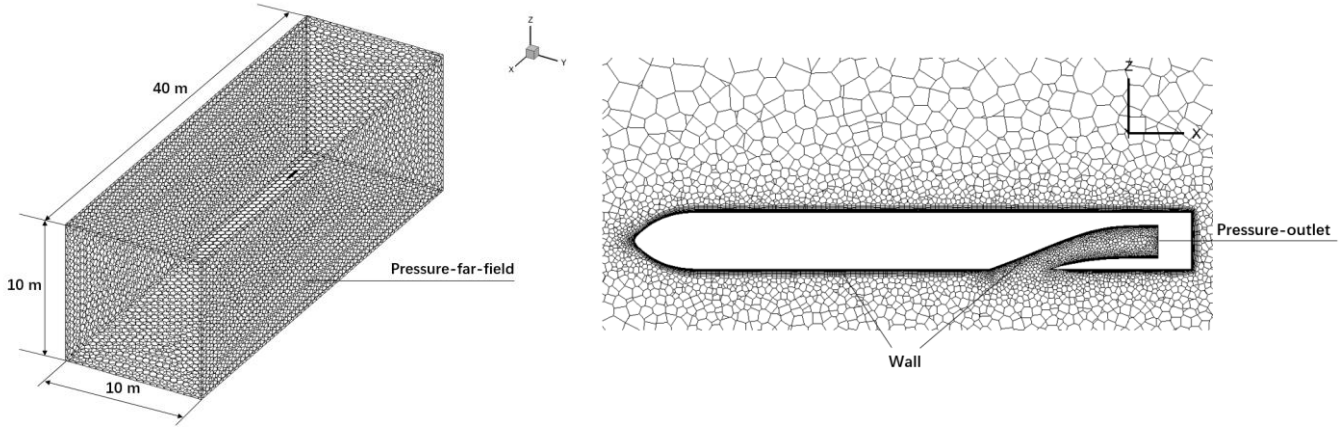

(**a**) (**b**)

Figure 2. Grid division and boundary conditions. (**a**) Computational domain grid. (**b**) Cross-section of the grid.

The total pressure recovery coefficient σ and the total pressure distortion index DI were used as the indexes to evaluate the performance of the inlet, which are defined as follows:

$$\sigma = P_m / P_\infty \tag{1}$$

$$DI = (P_{AIP,\max} - P_{AIP,\min}) / P_{FAV} \tag{2}$$

where P_m represents the flow weighted average total pressure on the exit of the inlet; P_∞ represents the total pressure of the incoming flow; $P_{AIP,\max}$ represents the maximum total

pressure on the exit of the inlet; $P_{AIP,\min}$ represents the minimum total pressure on the exit of the inlet; and P_{FAV} represents the average total pressure on the exit of the inlet.

For the purpose of guaranteeing the accuracy of the numerical calculation and saving calculation cost, it is necessary to verify the independence of the grid. Taking the baseline inlet as an example, the given calculation height is 5 km, the incoming flow Mach number M_0 is 0.73, the attack angle α is 2°, and the inlet exit's Mach number M_e is 0.37. By adjusting the node density of the surface grid of the object, four sets of grids are obtained. Their grid number and calculation results are shown in Table 1. Using the 5.71 million grid calculation results as reference, the errors of the 1.24 million and 3.32 million grid calculation results are less than 0.12%, indicating that the requirement of grid independence is met. Therefore, Scheme 2 is adopted for grid division in subsequent calculations.

Table 1. Grid scheme.

Grid Scheme	Number of Grids (Millions)	Total Pressure Recovery Coefficient σ	Error (%)	Total Pressure Distortion Index DI	Error (%)
1	0.86	0.9159	0.174	0.1735	1.225
2	1.24	0.9171	0.043	0.1712	0.116
3	3.32	0.9182	0.076	0.1715	0.058
4	5.71	0.9175	/	0.1714	/

2.3. Case Validation

Adopting the above numerical simulation and meshing method, the internal flow field of the baseline inlet configuration was simulated and compared with the relevant experimental data [5] to verify the reliability of calculation method used in this paper. The calculation conditions are given according to the experimental conditions, that is, the flight height is 5 km, the incoming Mach number M_0 is 0.73, the attack angle α is 2°, the sideslip angle β is 0°, and the inlet exit's Mach number M_e is 0.33~0.4. Table 2 shows the comparison between the total pressure recovery coefficient at different exits' Mach numbers obtained using experimental and calculated values. With the increase in the exit's Mach number, the total pressure recovery coefficient of the submerged inlet increases gradually. When the exit's Mach number is low, the separation vortex in the inlet channel increases, resulting in an increase in the relative error between the calculated value and the experimental value. In addition, the relative error is guaranteed to be less than 1%, which verifies the reliability of the numerical method.

Table 2. Comparison of total pressure recovery coefficients.

Exit Mach Number M_e	Total Pressure Recovery Coefficient σ		Relative Error (%)
	Experimental Values [5]	Simulation Values	
0.33	0.903	0.912	0.996
0.35	0.910	0.914	0.444
0.37	0.916	0.917	0.109
0.40	0.922	0.920	0.217

Figure 3 compares the total pressure recovery coefficient distribution contours of the inlet's exit section obtained using experiments [5] and numerical simulations when the inlet exit's Mach number is 0.4. It is manifest that the distribution position and area range of high and low total pressure areas at the inlet's exit obtained using wind tunnel experiments and numerical calculations are basically consistent, and the values are comparable. Therefore, the numerical simulation method which is used in this paper is reliable for the calculation of the internal flow of the submerged inlet.

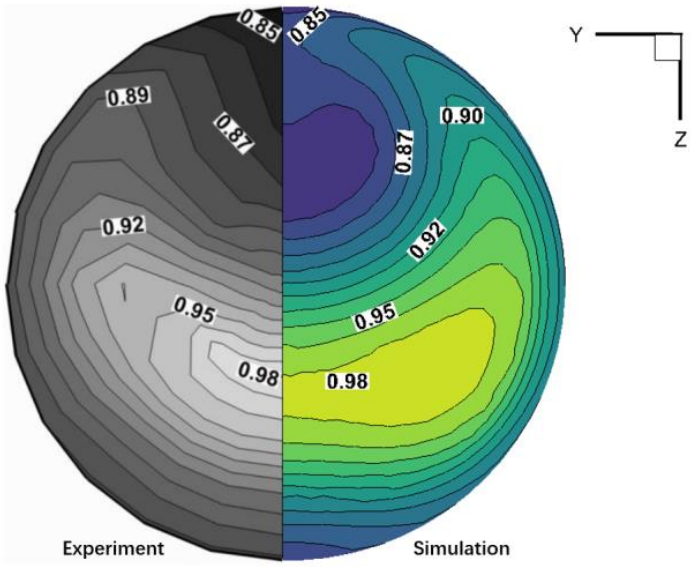

Figure 3. Comparison of total pressure recovery coefficient of the inlet's exit section.

3. Analysis of Internal Flow Characteristics of Submerged Inlet

The entrance of the submerged inlet is usually completely placed in fuselage or a projectile body, and therefore has no windward side, so it is difficult to use incoming flow stamping intake. As shown in Figure 4a, in the cruise state, except for a small number of streamlines away from the symmetry plane, the streamlines in front of the inlet enter the entrance's surface. In the meanwhile, as can be seen from Figure 4b, the streamlines on both sides of the inlet's entrance are bent, and significantly offset to the direction of the plane of symmetry, indicating that the side edge of the submerged inlet entrance's surface has the ability to suck in air, which is also one of the main intake modes of the submerged inlet. However, while enhancing the intake capacity, a large amount of low-energy boundary layer flow is sucked into the inlet and gradually develops, resulting in poor flow field quality of the inlet.

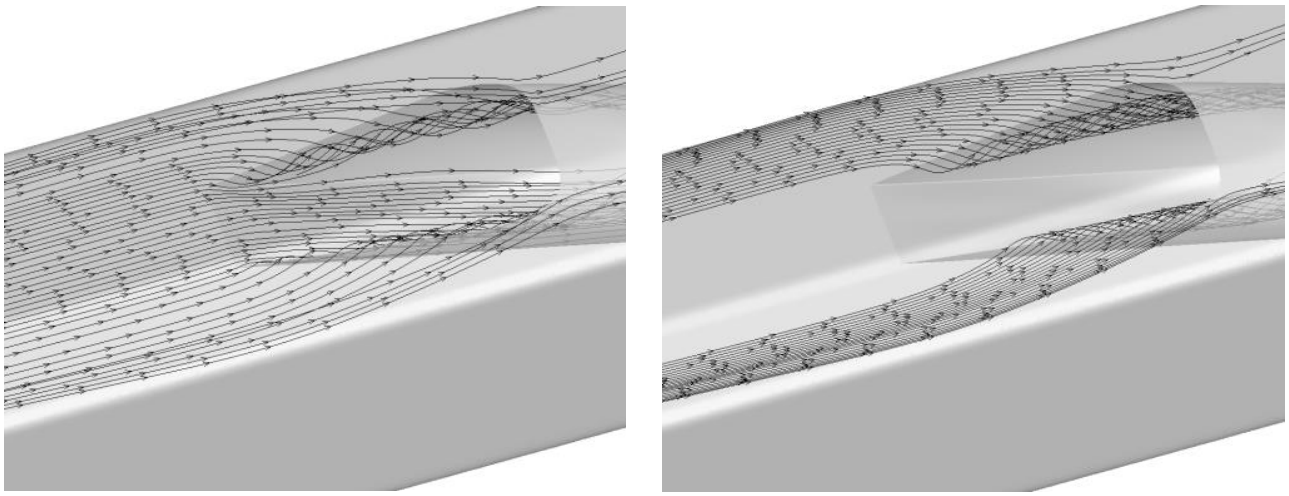

(**a**) (**b**)

Figure 4. Streamlines of submerged inlet's entrance under cruise condition. (**a**) Streamlines of the inlet's entrance (**b**) Streamlines on both sides of inlet's entrance.

In addition to the side-edge suction intake, as shown in Figure 5, there is a low-pressure area at the anterior lip of the submerged inlet, where the airflow expands and accelerates locally, and the local Mach number reaches 0.85, forming a pressure gradient perpendicular to the flow direction. This pressure gradient is also one of the driving forces for the airflow to turn into the inlet. Owing to the thick body boundary layer at the inlet's entrance, the low-energy airflow inevitably flows into the inlet, which decelerates the internal flow field and produces a large separation vortex, affecting the aerodynamic performance of the inlet.

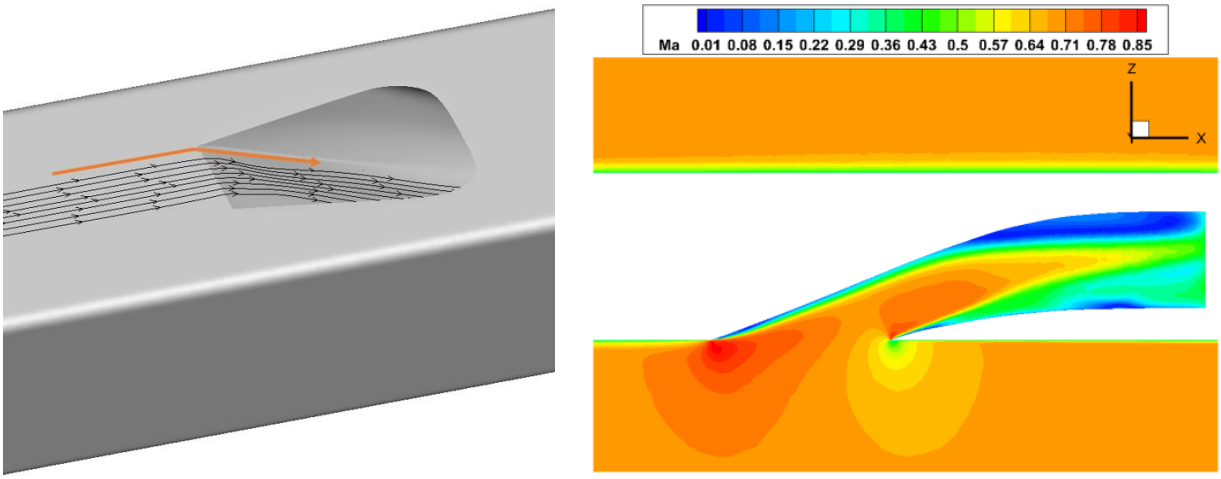

(**a**) (**b**)

Figure 5. Pressure gradient of the anterior lip of the submerged inlet. (**a**) Anterior lip pressure gradient. (**b**) Mach number contour of the symmetry plane.

As can be seen from Figure 6a, the low-energy boundary layer flows through the anterior lip diversion surface and the side-edge vortex suction into the inlet, and gradually develops and increases in the inlet channel. On the one hand, this is due to the development of the side-edge vortex itself. On the other hand, the transverse pressure difference from the upper wall to the lower wall is generated due to the bending of the inner channel, which makes some of the low-energy boundary layer flow of the upper wall boundary layer migrate to the lower wall. As the airflow enters the inlet, the area with the higher total pressure is concentrated in the center of the inlet channel, while the area with the lower total pressure always accumulates near the upper and lower sidewalls of the inlet. The vortex low-energy flow gradually accumulates near the symmetry plane under the action of a transverse pressure gradient and global swirl, and finally forms a large-scale low-total-pressure area dominated by the vortex below the inlet's exit. Due to the squeezing effect of the low total pressure area on the upper and lower walls, the high-total-pressure area is located in the upper half of the inlet's exit section with a small range, as shown in Figure 6b. The thick forebody boundary layer, the flow separation caused by the adverse pressure gradient on the lower wall, and the strong mixing loss of the side vortex lead to the low total pressure recovery coefficient of the submerged inlet and the large distortion of the exit flow field.

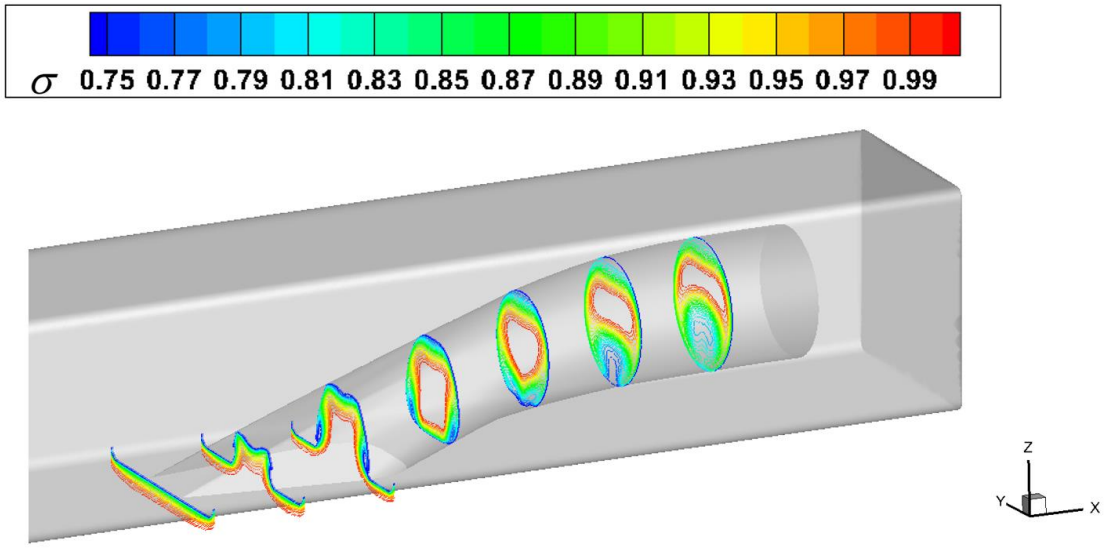

(**a**)

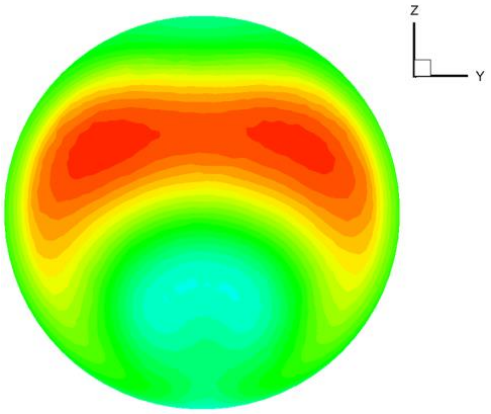

(**b**)

Figure 6. Total pressure recovery coefficient contours. (**a**) Total pressure recovery coefficient contour of the inlet section along the path. (**b**) Total pressure recovery coefficient contour of the inlet's exit.

4. Design of Synergistic Bulge Submerged Inlet and Internal Flow Characteristics Analysis

4.1. Design Principle of Prepositive Synergistic Bulge for Submerged Inlet

One of the main reasons for the low total pressure recovery coefficient is that the submerged inlet inhales the low-energy forebody boundary layer. Therefore, a direct idea to improve the performance of the submerged inlet is to effectively deal with the boundary layer before the inlet to improve the overall intake efficiency and aerodynamic performance. In this paper, a passive flow control method is proposed to improve the performance of the inlet by adding a synergistic bulge on the surface of the projectile upstream of the inlet's entrance. The design requirements of this configuration include the following: (1) It can effectively deal with the low-energy boundary layer before the entrance of the inlet and improve the entrance air quality of the submerged inlet. (2) It does not change the original intake mode of the inlet and does not reduce the intake air volume. (3) The benefit of improving the inlet's performance is greater than the negative effect of increasing the additional drag of the aircraft after adding the bulge.

Combined with the above design requirements and the analysis of the internal flow characteristics of the baseline inlet, the added bulge should mainly deal with the air flow in the red frame of Figure 7a, without affecting the entrainment intake of the side edge of the inlet's entrance. Therefore, the position of the bulge is set at the junction of the projectile's surface and the anterior lip of the inlet, and the bottom shape is set to be square. As shown in Figures 7b and 8, compared with the baseline inlet, the curvature radius of the local surface in front of the anterior lip of the inlet with a bulge is reduced. The airflow is blocked by the bulge when it flows to the windward side of the bulge, and the speed is reduced, which is beneficial to promote the negative pressure suction of the inlet. When it flows through the leeward side of the bulge, it is equivalent to a flow downstream to the slope, the airflow is accelerated, and the energy is injected into the boundary layer. At the same time, the bulge diverts a small amount of low-energy flow of the forebody boundary layer away from the inlet's entrance, prevents the separation of the downstream boundary layer of the anterior lip, and the aerodynamic performance of the submerged inlet is improved.

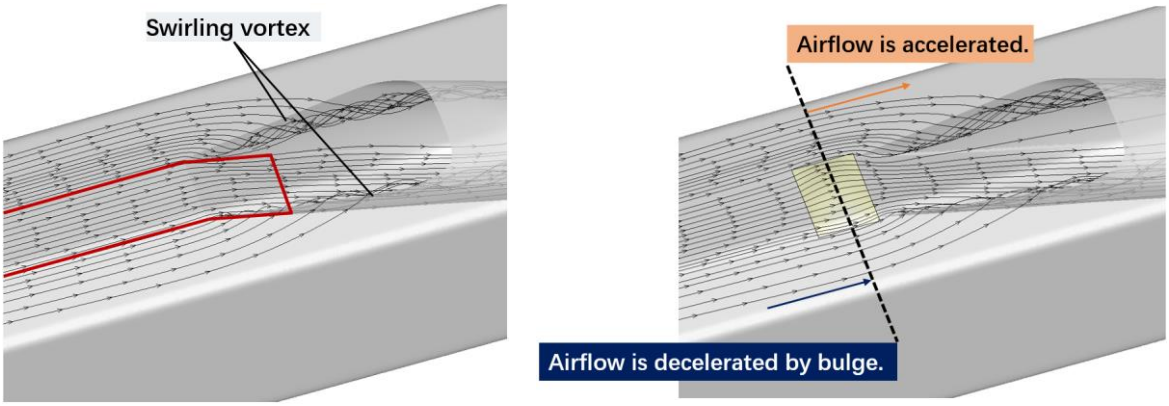

(**a**) (**b**)

Figure 7. Prepositive synergistic bulge design for submerged inlet. (**a**) Bulge effective position. (**b**) Bulge efficiency way.

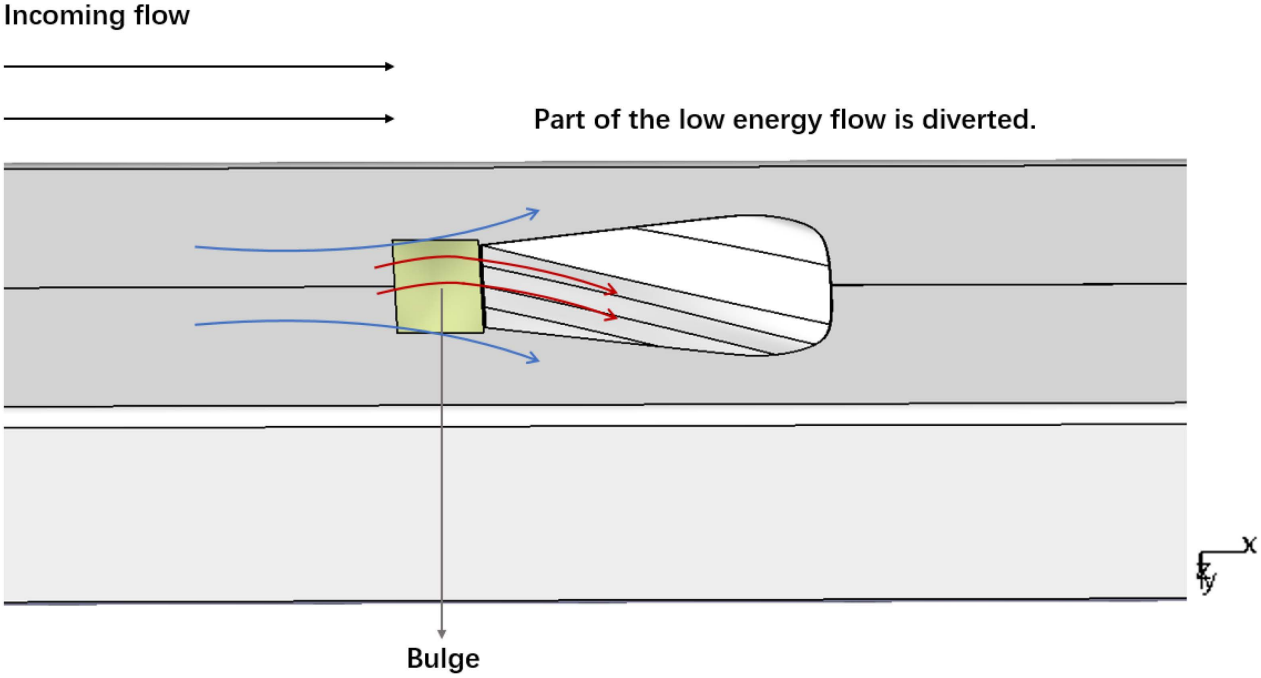

Figure 8. *Cont.*

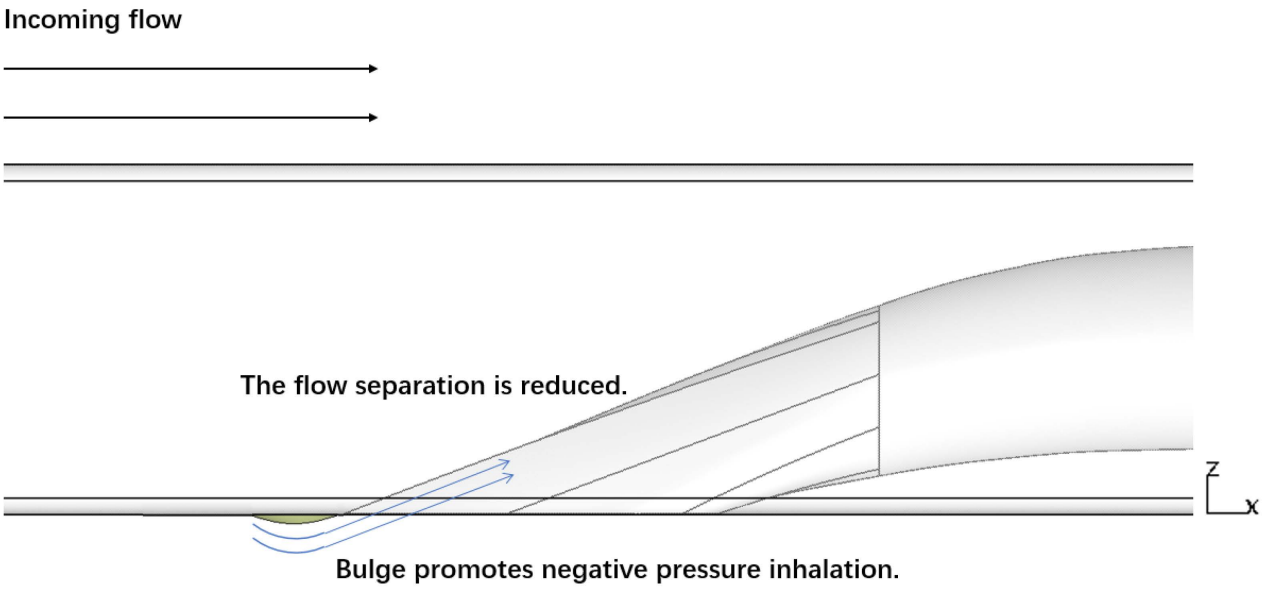

Figure 8. Design principle of prepositive synergistic bulge.

Moreover, after adding the bulge, additional drag will be caused by factors such as friction of the fluid flowing through the bulge. Therefore, the drag around the projectile in the baseline configuration should be compared with the drag around the bulge and the projectile in the new configuration. In order to measure whether the negative effect caused by the increase in drag is acceptable for the whole projectile body and the inlet system, the change in the flow-weighted average total pressure at the exit of the inlet is used as a reference to limit the increase in the drag around the projectile and the bulge compared to the drag of the baseline configuration. When the average total pressure of the inlet's exit in the synergistic bulge inlet configuration is increased by 1% compared with that of the baseline inlet configuration, the drag around the projectile and the bump can be increased by 1% at most. To ensure that the benefit of the inlet performance improvement obtained by adding the bulge is greater than the loss caused by the additional drag to the entire system, we use:

$$\frac{(D_b - D_0)P_{AIP,0}}{(P_{AIP,b} - P_{AIP,0})D_0} \leq 1 \tag{3}$$

where D_0 represents the drag around the projectile in the baseline configuration; D_b represents the drag around the projectile and the bulge in the synergistic bulge inlet configuration; $P_{AIP,0}$ represents the baseline inlet exit's flow-weighted average total pressure; $P_{AIP,b}$ represents the synergistic bulge inlet exit's flow-weighted average total pressure.

The prepositive synergistic bulge inlet configuration contains three design parameters: The ratio of the bulge width to the inlet's anterior lip width L_y/L_{lip}, the aspect ratio L_x/L_y, and the height Δz of the bulge, as shown in Figure 9. The shape of the synergistic bulge is defined by a series of point coordinates (x_b, y_b, z_b). Here, x_b, y_b can be determined using the inlet's entrance position and the range of the length L_x and width L_y of the bulge, and z_b is defined using Equation (4). The initial point (x_0, y_0, z_0) is located on the surface of the projectile, which can be obtained using the design parameters of the bulge and the position of the lower surface of the projectile.

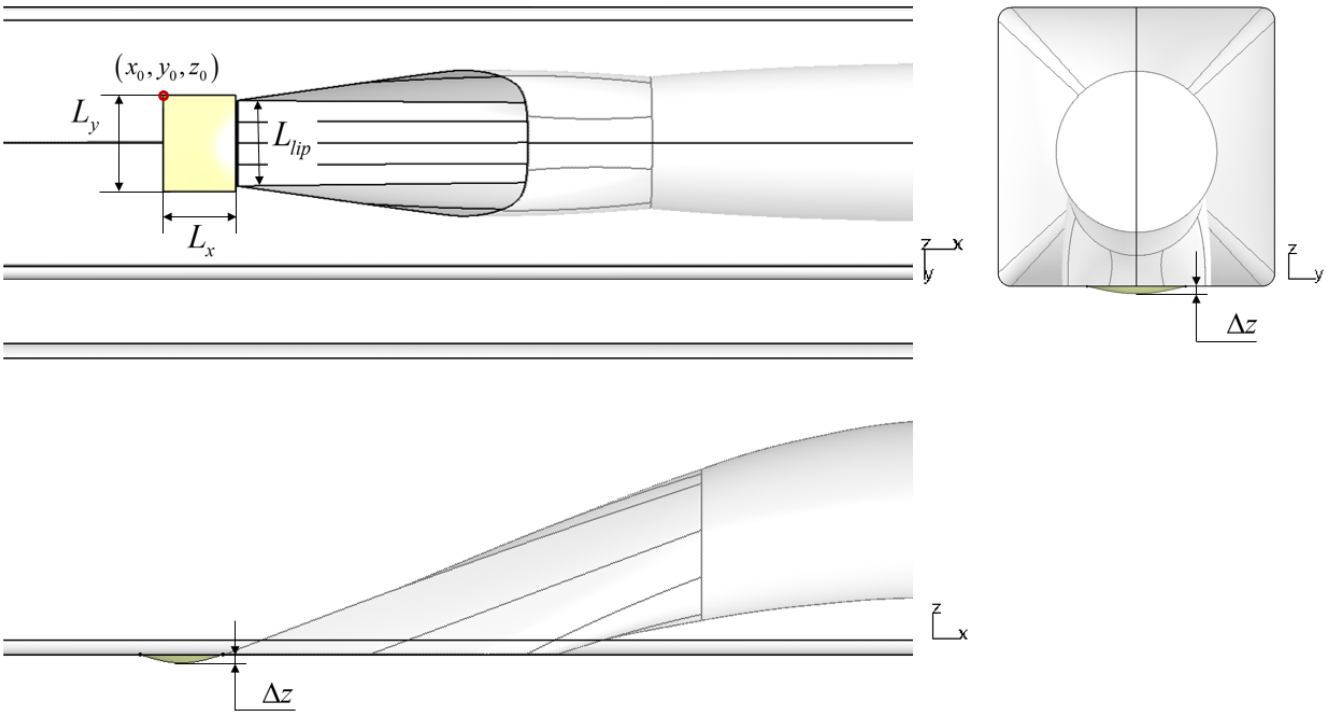

Figure 9. Design parameters of prepositive synergistic bulge inlet configuration.

$$z_b = z_0 - \Delta z \sin \frac{(x_b - x_0)\pi}{L_x} \sin \frac{(y_b - y_0)\pi}{L_y} \tag{4}$$

4.2. Comparison of Internal Flow Characteristics of Submerged Inlet with or without Synergistic Bulge

The synergistic bulge is set in front of the baseline inlet, and the parameters are selected as $L_y/L_{lip} = 1.1$, $L_x/L_y = 0.75$, and $\Delta z = 3$ mm, that is, the bulge is slightly wider than the anterior lip of the inlet. The new configuration is calculated and compared with the baseline inlet to analyze its aerodynamic performance and its influence on the drag of the projectile body.

The comparison of the aerodynamic performance parameters between the baseline inlet configuration and the synergistic bulge inlet configuration at different exit Mach numbers is shown Figure 10. After setting the synergistic bulge, the total pressure recovery coefficient of the baseline inlet is increased by up to 1.36%, while the total pressure distortion index is reduced by 10.86%. Furthermore, it is easy to find that when the exit Mach number is smaller, the improvement influence of the prepositive synergistic bulge inlet configuration on the inlet performance is more obvious. The drag of the projectile increases from 79.379 N to 79.678 N, with an increase of 0.37%, which meets the design requirements.

Figure 11 compares the total pressure on the exit surface of the baseline inlet configuration and the synergistic bulge inlet configuration at different exit Mach numbers. The high total pressure area on the inlet exit's surface is obviously enlarged due to the existence of the bulge, which covers a small low-pressure area above the baseline inlet's exit, and the low total pressure area below the inlet exit's surface is also slightly reduced, thus increasing the average total pressure on the inlet exit's surface, and also increasing the total pressure recovery coefficient and decreasing the total pressure distortion index. The bulge accelerates the airflow by pushing away part of the low-energy boundary layer to eliminate the flow separation in the inlet and increases the total pressure on the inlet's exit. In particular, the total pressure of a low-pressure area above the exit is greatly increased to form a large high-pressure area, thereby improving the performance of the inlet. When the

inlet exit's Mach number becomes larger, the range of low total pressure area above the baseline inlet's exit is smaller. At this time, the role of the synergistic bulge can be limited, so its effect on improving the inlet's performance gradually deteriorates. In other words, under a low exit Mach number, the bulge can have a stronger effect. Additionally, the existence of the bulge does not have a negative impact on the performance of the inlet.

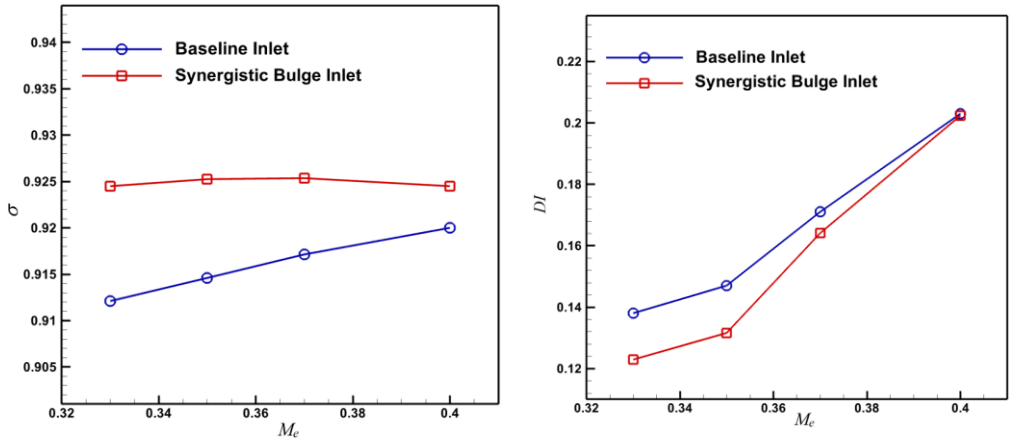

(**a**) (**b**)

Figure 10. Comparison of inlet performance parameters. (**a**) Total pressure recovery coefficient. (**b**) Total pressure distortion index.

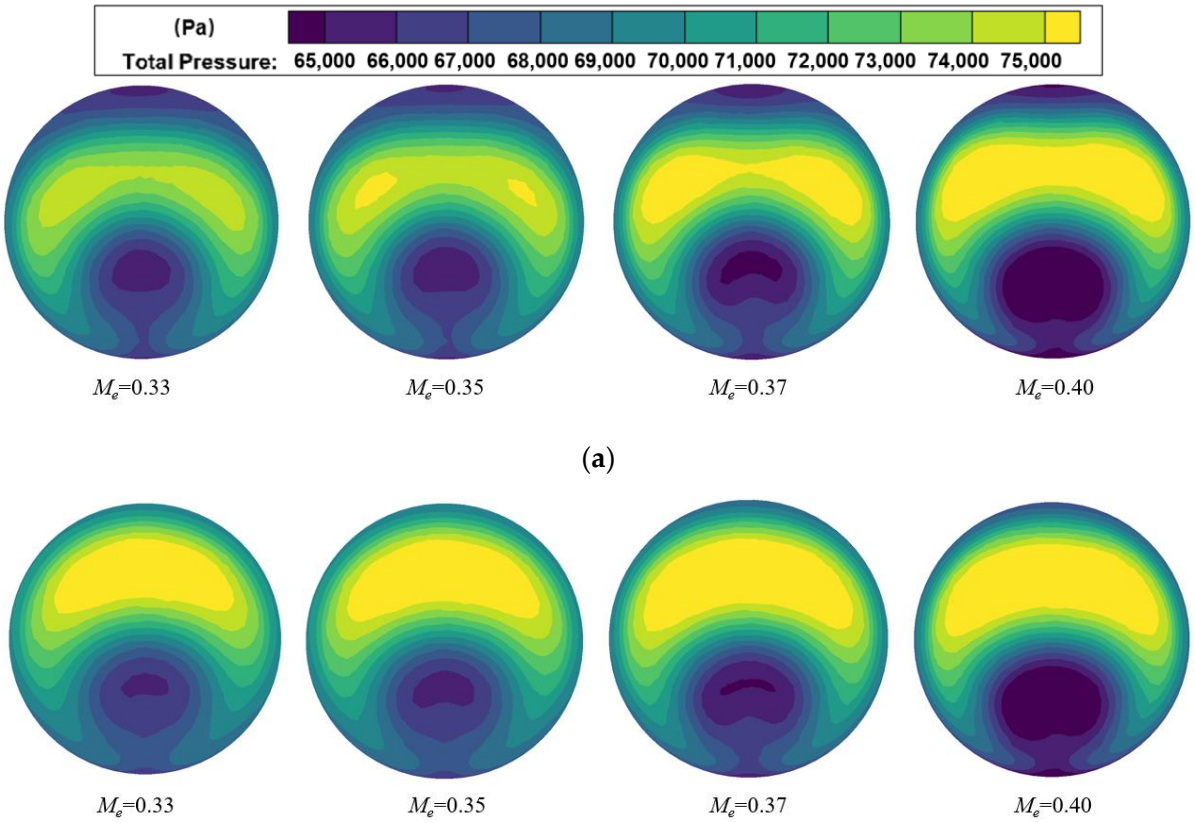

(**a**)

(**b**)

Figure 11. Comparison of the total pressure of the inlet's exit at different exit Mach numbers. (**a**) Total pressure of the baseline inlet's exit. (**b**) Total pressure of the synergistic bulge inlet's exit.

Figure 12 shows the pressure contours of the object surface near the inlet entrance of the baseline inlet and the synergistic bulge inlet when Me = 0.37. It can be seen that there is a high-pressure area on the windward side of the bulge, and the spanwise pressure difference is beneficial to push the low-energy boundary layer flow to both sides of the bulge. At the anterior lip of the inlet, the pressure along the center line is significantly increased. And the range of the low-pressure area in the channel near the inlet's entrance is increased, which is helpful for the negative pressure suction of the inlet.

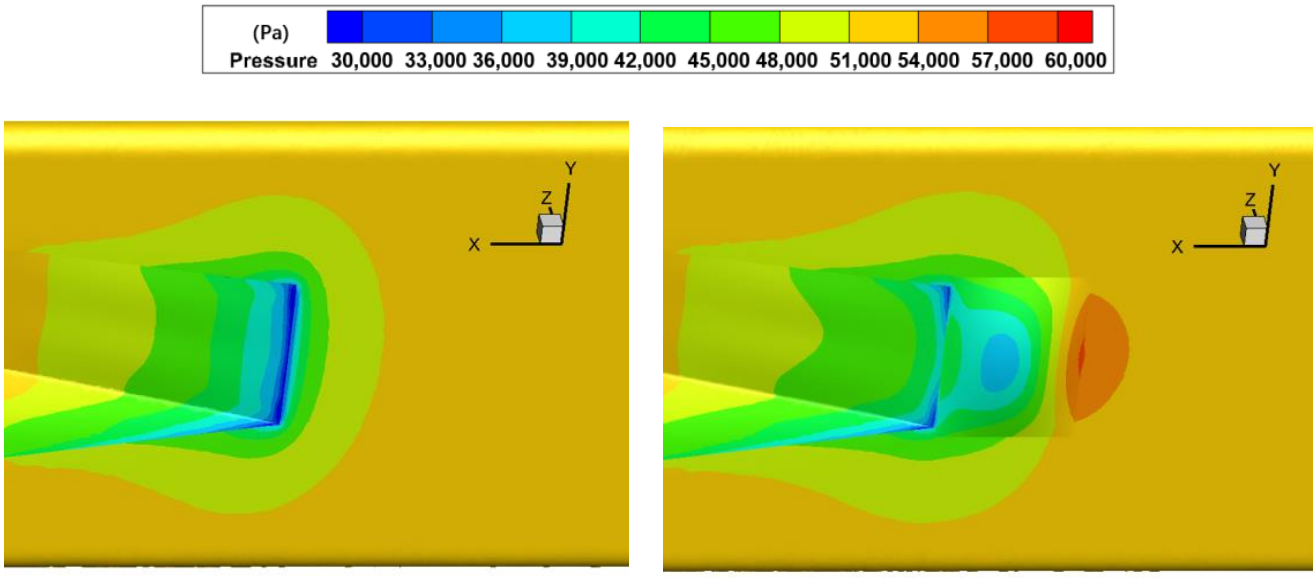

(**a**) (**b**)

Figure 12. Pressure contours near the inlet's entrance surface (Me = 0.37). (**a**) Baseline inlet (**b**) Synergistic bulge inlet.

Figure 13 selects the streamline contours of the internal flow field and the velocity contours of the symmetrical section of the inlet with the exit Mach number which is 0.33 and 0.4 for analysis. When the fluid flows through the bulge, it is decelerated on the windward side of the bulge and accelerated into the inlet on the leeward side. The existence of the bulge causes a part of low-energy boundary layer on the projectile's body to stay away from inlet's entrance and there is a large speed increase on the wall near the anterior lip inside the inlet, these eliminating the separation vortex formed by low-energy fluid in the baseline inlet, and increasing the total pressure on the inlet exit's surface.

In Figure 13b, the existence of the bulge augments the secondary flow, thus forming a relatively low velocity area at the end of the synergistic bulge inlet for Me = 0.33. In order to judge whether the swirl distortion of the synergistic bulge inlet is acceptable, the swirl angle α_s is used as the evaluation index, which is defined as Equation (5) [32].

$$\alpha_s = \arctan(U_\theta / U_x) \tag{5}$$

where U_θ represents the circumferential velocity component at a certain point on the inlet's exit; U_x represents the axial velocity component at a certain point on the inlet's exit.

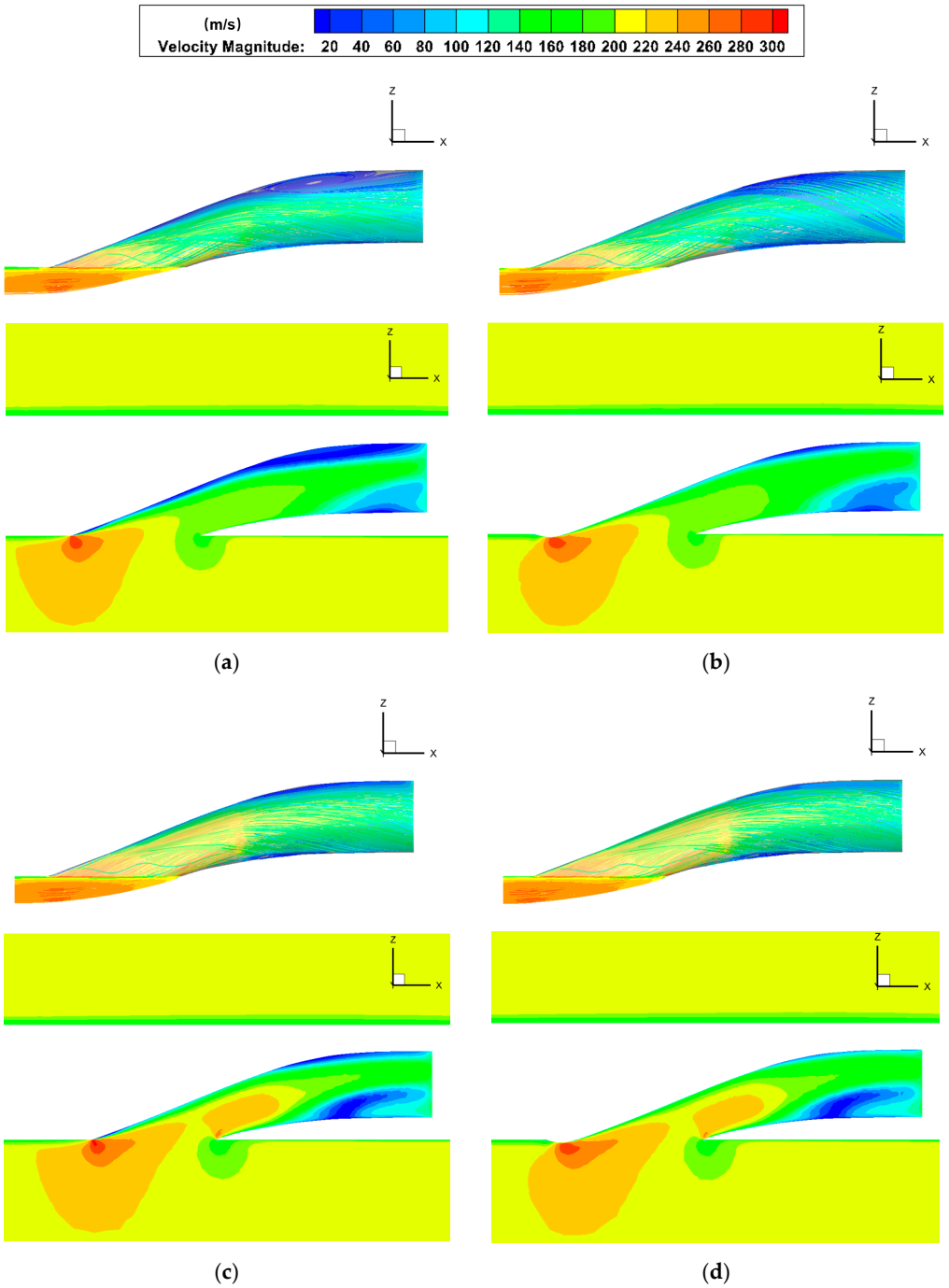

Figure 13. Inlet internal streamline contours and symmetrical section velocity contours. (**a**) Baseline inlet (Me = 0.33). (**b**) Synergistic bulge inlet (Me = 0.33). (**c**) Baseline inlet (Me = 0.40). (**d**) Synergistic bulge inlet (Me = 0.40).

Figure 14 shows the comparison of swirl angles between the baseline inlet's exit and the synergistic bulge inlet's exit at different exit Mach numbers. The swirl angles on the exit's surface show a horizontal symmetric distribution, and the swirl is in a counter-rotating mode. The large swirl angles are concentrated in the lower half of the exit, and the swirl angle of the outer ring reaches 20°. There are also symmetrical small swirl angles in the upper part of the exit of the baseline inlet, and the absolute value of the angles decreases with the increase in the exit Mach number, while the range of the large swirl angles in the lower part increases with the increase in the exit Mach number. The exit of the synergistic bulge inlet has only large swirl angles in the lower part, which is similar to the baseline

inlet, and the swirl angles are almost unchanged with the change in exit Mach number. By comparing the swirl angles, it can be assumed that the swirl distortion of the synergistic bulge inlet is acceptable.

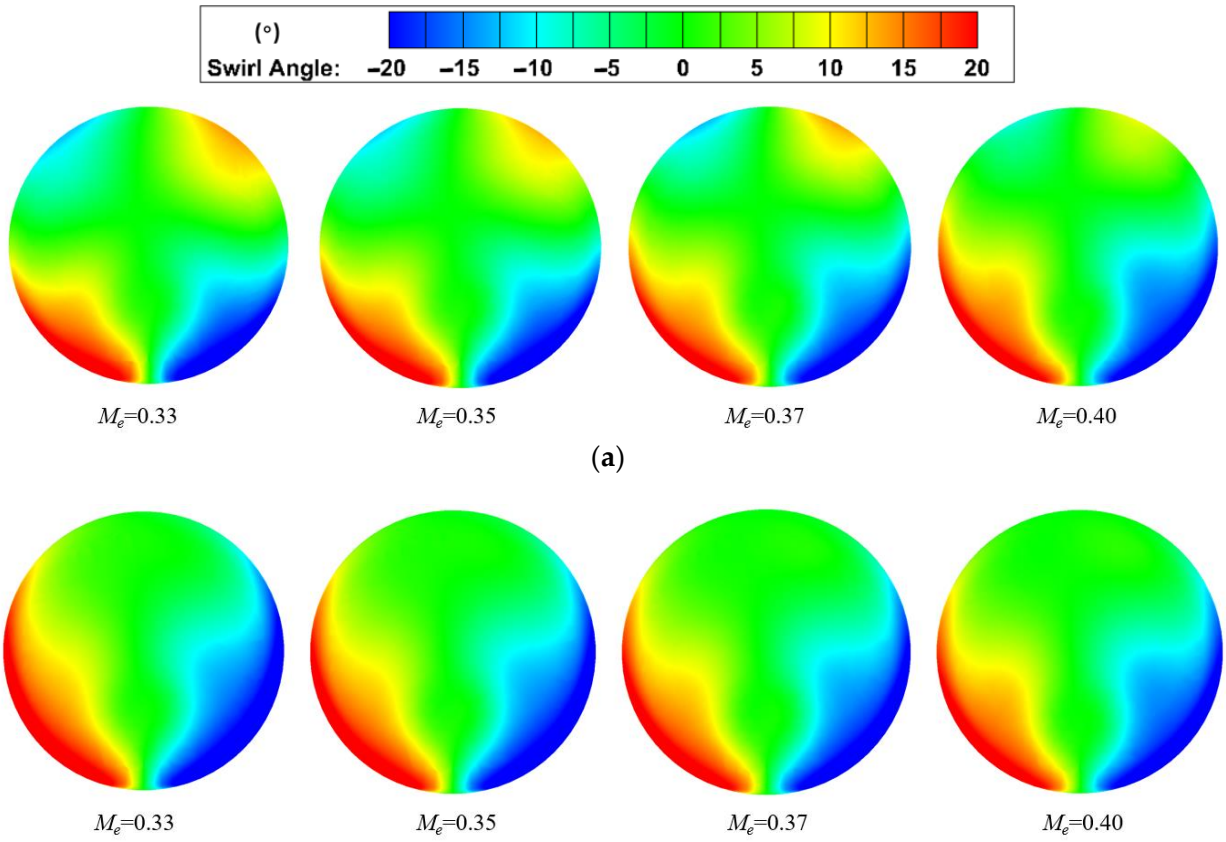

Figure 14. Comparison of swirl angles of the inlet's exit at different exit Mach numbers. (**a**) Swirl angles of the baseline inlet's exit. (**b**) Swirl angles of the synergistic bulge inlet's exit.

4.3. Analysis of the Influence of Synergistic Bulge Design Parameters

With the purpose of further clarifying the influence of design parameters on the performance of the inlet, the control variable method is used to change the three parameters' values on the basis of $L_y/L_{lip} = 1.1$, $L_x/L_y = 0.75$, and $\Delta z = 3$ mm, and different prepositive synergistic bulge inlet configurations are calculated. The values of each design parameter are shown in Table 3. Moreover, some of the synergistic bulge configurations with different design parameters are shown in Figure 15.

Table 3. The values of design parameters.

Ratio of the Width of the bulge to the width of the inlet's anterior lip L_y/L_{lip}	0.2	0.5	0.8	1	1.1	1.4
The aspect ratio of the bulge L_x/L_y	0.25	0.5	0.75	1		1.25
The height of the bulge Δz (mm)	1	2	3	4		5

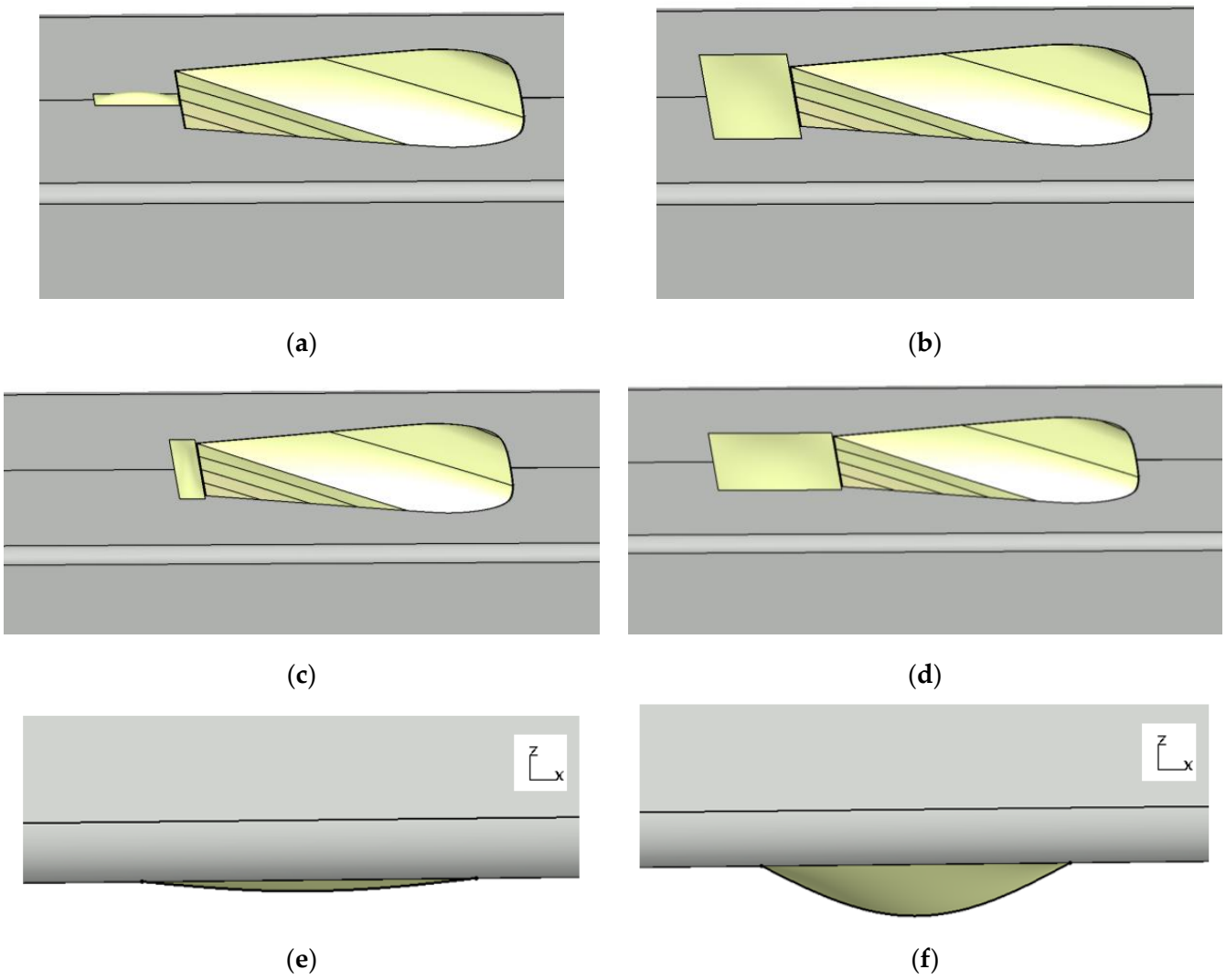

Figure 15. Different design parameters of synergistic bulge configurations. (**a**) L_y/L_{lip} = 0.2. (**b**) L_y/L_{lip} = 1.4. (**c**) L_x/L_y = 0.25. (**d**) L_x/L_y = 1.25. (**e**) Δz = 1 mm. (**f**) Δz = 5 mm.

Figures 16–18 show the influence of three design parameters, respectively, on the total pressure recovery coefficient and the total pressure distortion index of different inlet configurations. Except for the configuration with the aspect ratio $L_x/L_y = 0.25$ of the bulge, the aerodynamic performance of the synergistic bulge inlet configurations is improved compared with the baseline inlet configuration, which also indicates that the prepositive synergistic bulge configuration has the advantage of a high fault tolerance rate in design and use. In the calculated configurations, the additional drag brought by the bulge to the projectile basically increases with its height, but the increase is small and within the acceptable range. When the bulge height is 5 mm, the drag is the largest, with an increase of 0.86% compared with the baseline model.

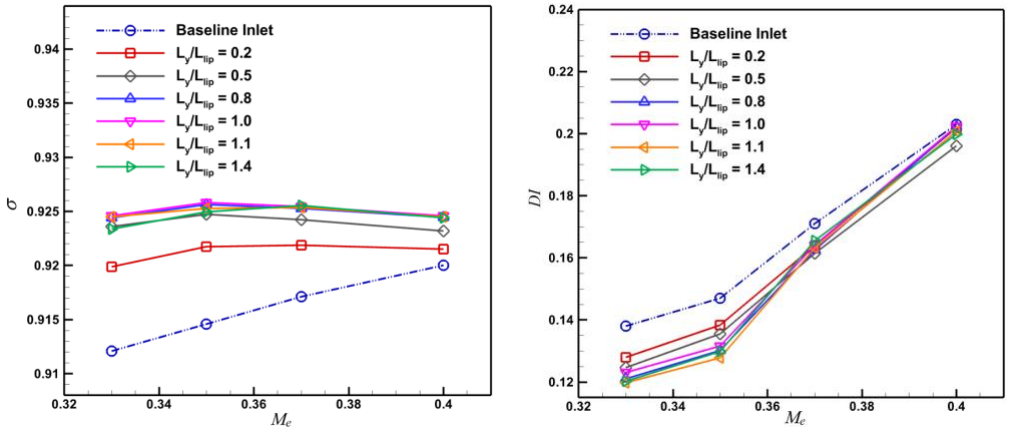

Figure 16. Effect of the ratio of the bulge width to the width of the inlet's anterior lip on inlet performance. (**a**) Total pressure recovery coefficient. (**b**) Total pressure distortion index.

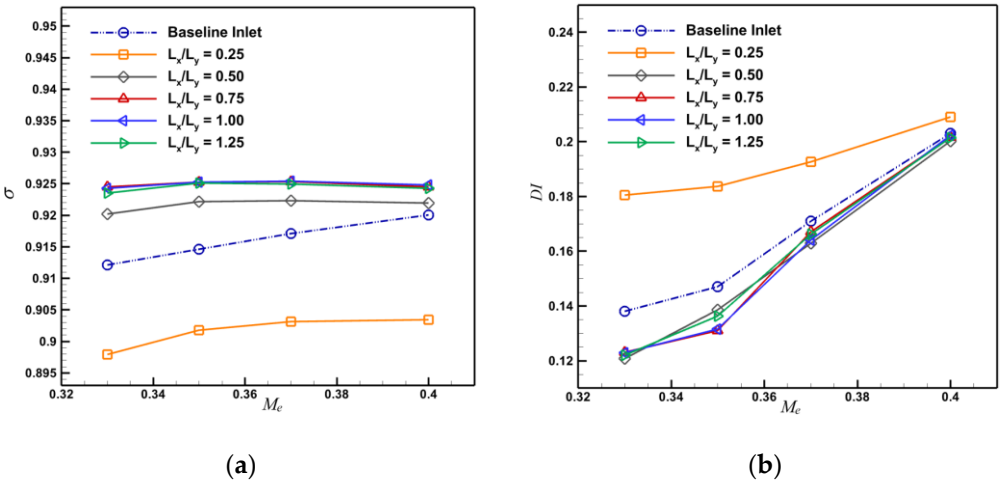

Figure 17. Effect of the bulge aspect ratio on inlet performance. (**a**) Total pressure recovery coefficient. (**b**) Total pressure distortion index.

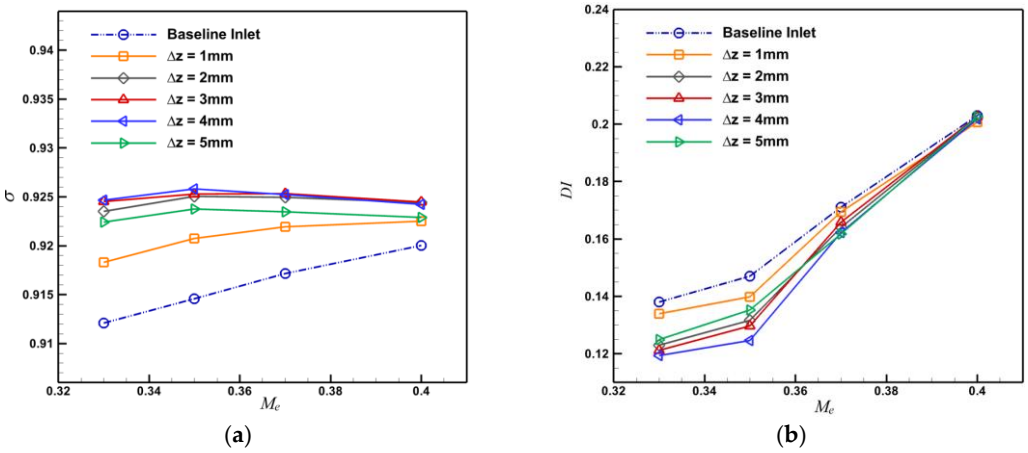

Figure 18. Effect of the bulge height on inlet performance. (**a**) Total pressure recovery coefficient. (**b**) Total pressure distortion index.

According to the calculation results, the width of the bulge should be at least half of the width of the inlet's anterior lip, and a height of the bulge between 2 and 4 mm is more appropriate. When the bulge is wider than the anterior lip of the inlet ($L_y/L_{lip} > 1$), it will not cause negative airflow interference, and when the bulge is much smaller than the width of the anterior lip, such as $L_y/L_{lip} = 0.2$, it can still play a certain role in improving aerodynamic performance. This shows that the method of setting a synergistic bulge in front of the inlet's entrance is mainly effective along the center line of the bulge. Figure 19 shows the streamline diagrams of the symmetrical section of the synergistic bulge inlets with $\Delta z = 4$ mm and $\Delta z = 5$ mm at Me = 0.37. As the height of the bulge Δz increases to 5 mm, flow separation occurs after the bulge, which leads to a decrease in the effect of the bulge on improving the performance of the inlet. Among the three design parameters, the aspect ratio of the bulge L_x/L_y has the greatest impact on the performance of the inlet. As shown in Figure 20, the total pressure of the symmetrical section of the projectile with a submerged inlet in which the synergistic bulge's aspect ratio are $L_x/L_y = 0.25$ and $L_x/L_y = 0.75$, respectively, and the baseline inlet is compared under the condition that inlet exit's Mach number $M_e = 0.37$. Due to the small aspect ratio of the bulge, not only the low-energy boundary layer at the inlet's entrance is partially excluded, but also a low-pressure area is formed after the bulge, which seriously reduces the inlet's performance. Therefore, the aspect ratio of the bulge should be above 0.75. It can also be said that the increase in the curvature of projectile surface in front of the inlet's anterior lip is conducive to improving the performance of the inlet, but when the curvature value is designed too large, it will have a negative impact.

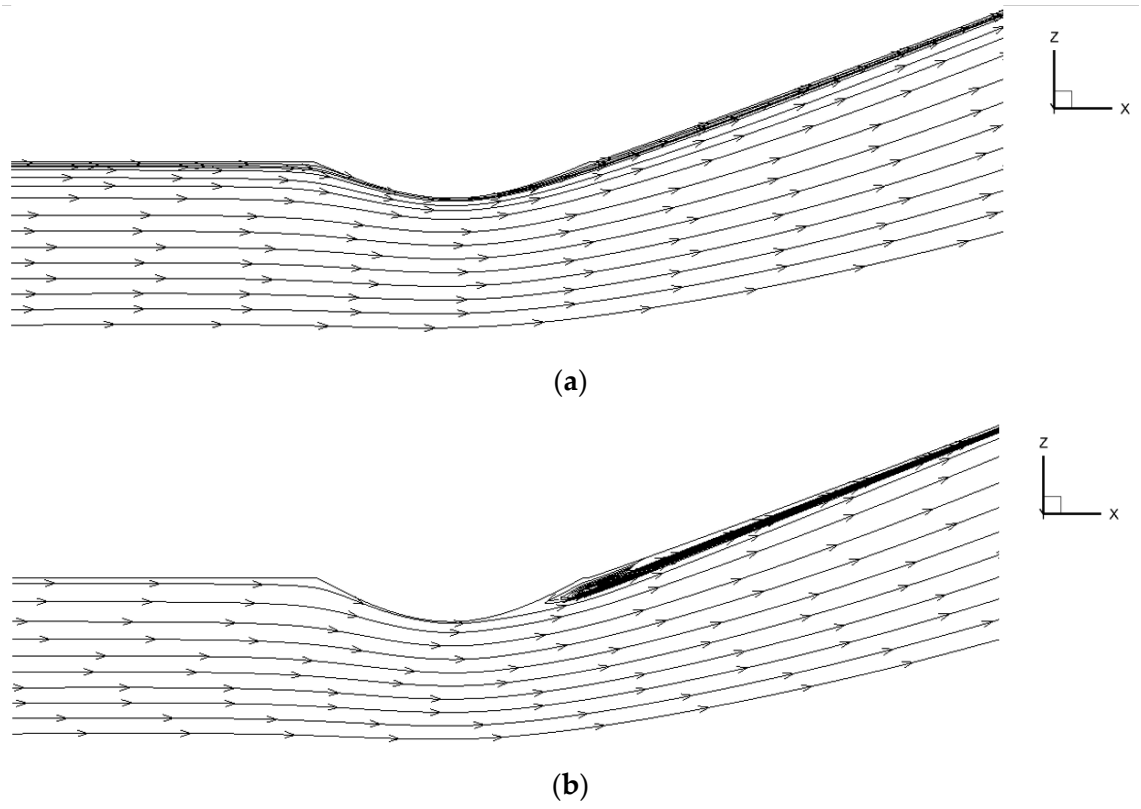

Figure 19. Streamline diagrams of the symmetrical section ($M_e = 0.37$). (**a**) $\Delta z = 4$ mm. (**b**) $\Delta z = 5$ mm.

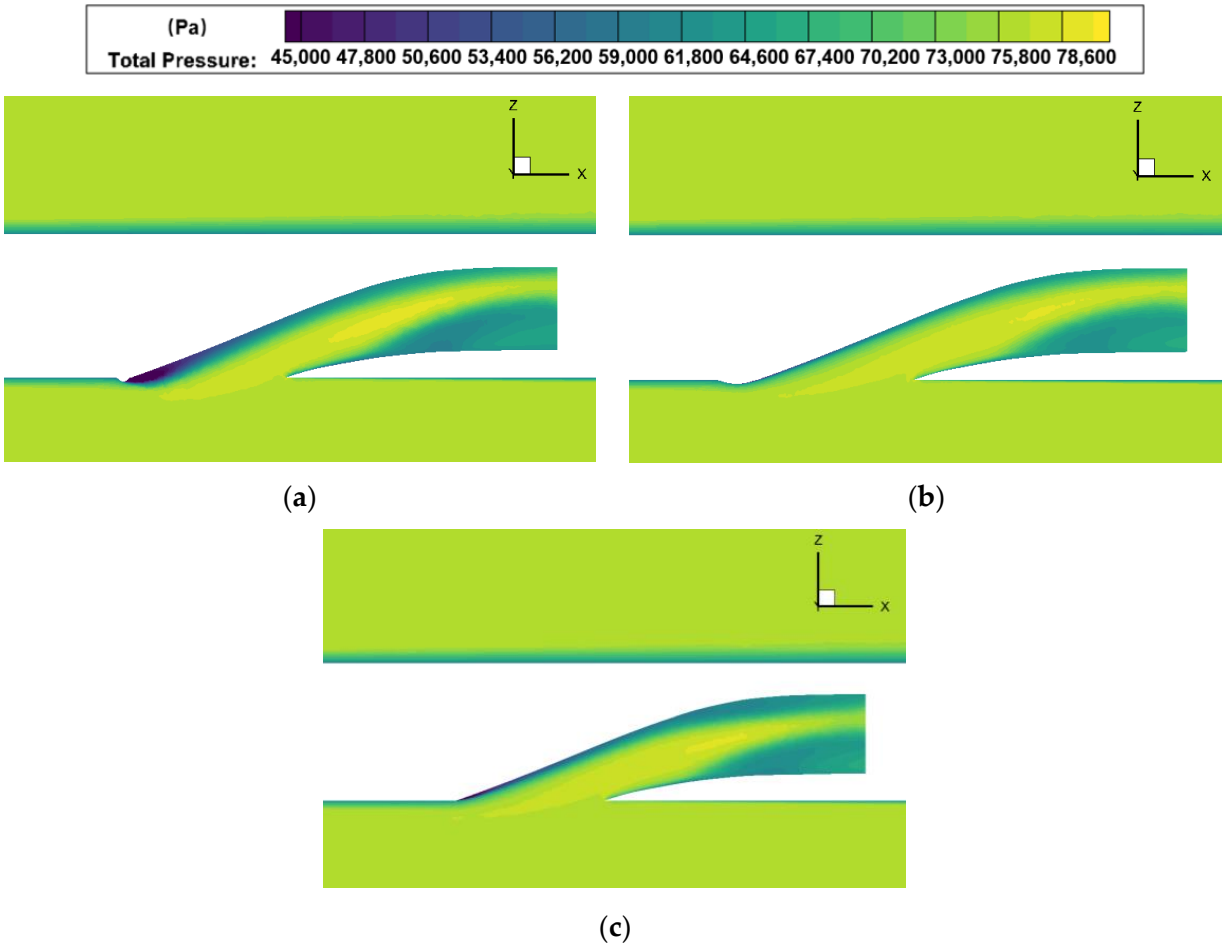

Figure 20. Total pressure contours of the symmetrical section (M_e = 0.37). (**a**) L_x/L_y = 0.25. (**b**) L_x/L_y = 0.75. (**c**) Baseline inlet.

5. Applicability Evaluation of Internal and External Flow Interference Effect of Prepositive Synergistic Bulge Inlet

An exit Mach number of M_e = 0.37 is selected to calculate the performance parameters of the prepositive synergistic bulge inlet configuration under different incoming Mach numbers M_0, attack angles α, and sideslip angles β and compare them with the aerodynamic performance parameters of the baseline inlet configuration. Meanwhile, the increase in drag of the projectile after adding the bulge under each state is calculated to verify whether it meets the design requirements. And then, the applicability of the prepositive synergistic bulge inlet configuration to the internal and external flow under different flight conditions is evaluated.

Figure 21 shows the calculation results of two inlet configurations at Mach numbers of M_0 = 0.43~0.83. The synergistic bulge has a positive effect on improving the performance of the baseline inlet within the calculated range. With the increase in the incoming Mach number, the total pressure recovery coefficients of two inlet configurations gradually decrease, and the total pressure distortion indices increase. In this situation, the space for improving the aerodynamic performance of the baseline inlet increases, and the effect of the synergistic bulge becomes more significant. In addition, the drag of the projectile body increases with the increase in the incoming Mach number. The drag increase ratio after adding the bulge is calculated according to Equation (3) and the computation results are shown in Figure 22. Except for the condition of M_0 = 0.43, the increase in drag in the other conditions is within the allowable range for the design, which indicates that this configuration cannot achieve good results at low flight speed. This is mainly due

to the improvement of the internal flow, which is caused by the synergistic bulge, being too small. In fact, when M_0 = 0.43, the drag of the projectile only increases by 0.07% and the cruise speed of the subsonic projectile is generally greater than 0.6 Mach. Therefore, it can be assumed that the prepositive synergistic bulge inlet configuration is practical in engineering.

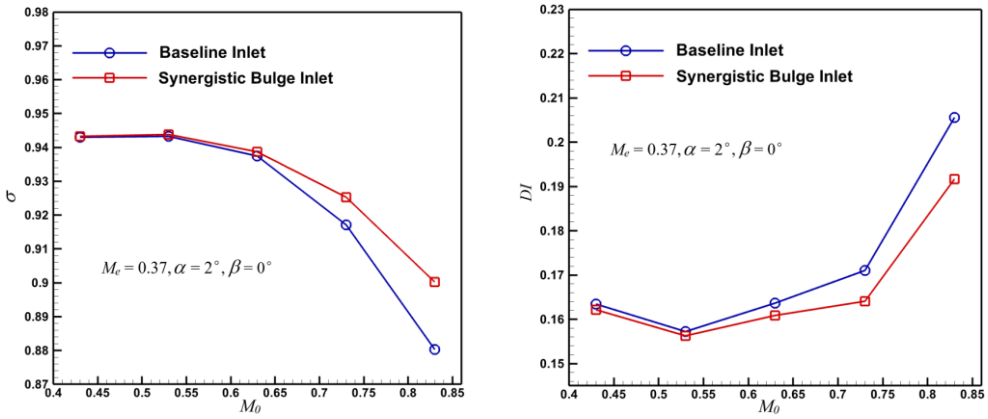

Figure 21. Comparison of inlet performance at different incoming Mach numbers. (**a**) Total pressure recovery coefficient. (**b**) Total pressure distortion index.

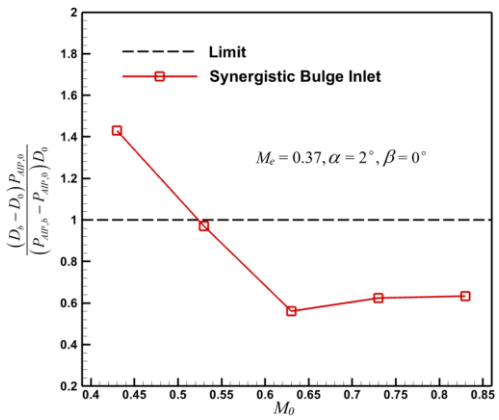

Figure 22. Drag increases at different incoming Mach numbers.

Figures 23–26 show a comparison of the aerodynamic performance parameters of the baseline inlet configuration and the synergistic bulge inlet configuration calculated under the conditions of attack angles of $\alpha = -2°$~$8°$ and sideslip angles of $\beta = 0°$~$8°$, as well as the increase in the proportion of the projectile's drag. Compared with the baseline inlet, the synergistic bulge inlet configuration has the effect of improving the total pressure recovery coefficient and reducing the total pressure distortion index under the calculation states of multiple attack angles and sideslip angles. And the ratio of the increase in the projectile's drag to the average total pressure increase increment at the inlet's exit can meet the condition of less than 1%. In general, from the perspective of both internal and external flow, the method of adding the prepositive synergistic bulge in front of the submerged inlet to improve the inlet performance has wide applicability.

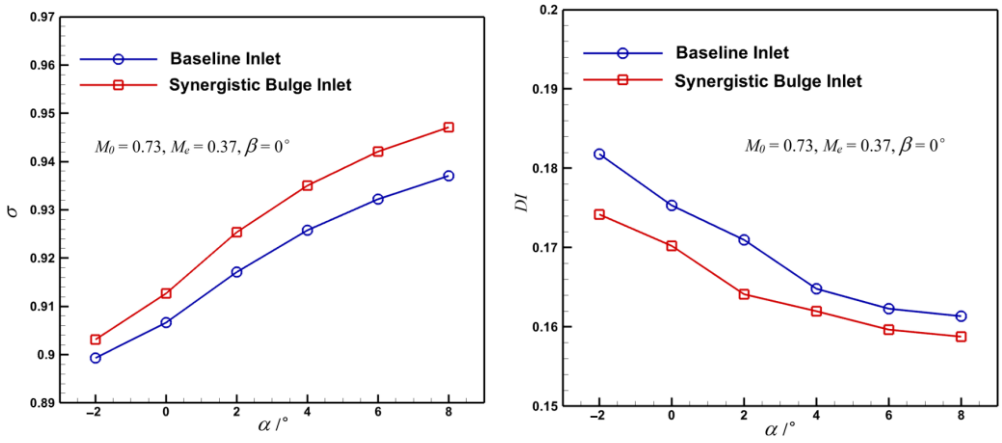

Figure 23. Comparison of inlet performance at different angles of attack. (**a**) Total pressure recovery coefficient. (**b**) Total pressure distortion index.

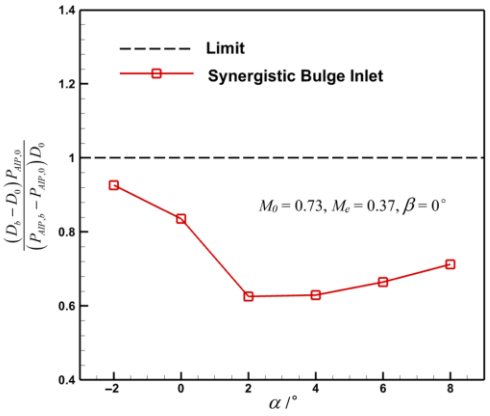

Figure 24. Drag increases at different angles of attack.

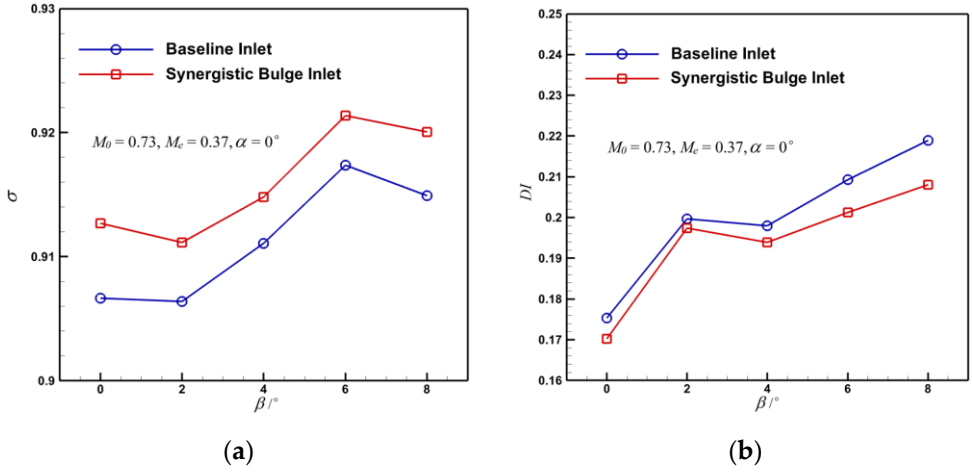

Figure 25. Comparison of inlet performance at different sideslip angles. (**a**) Total pressure recovery coefficient. (**b**) Total pressure distortion index.

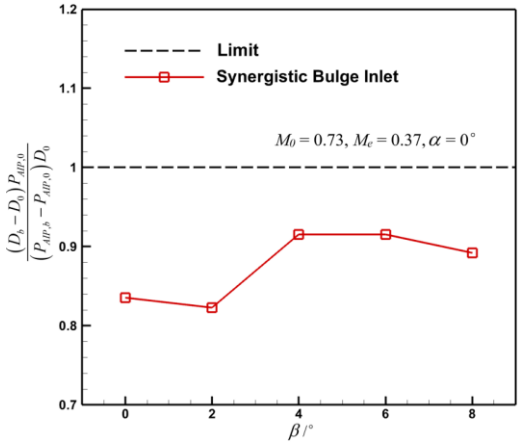

Figure 26. Drag increases at different sideslip angles.

6. Conclusions

According to the basic flow field characteristics of the submerged inlet, a method for improvement in the aerodynamic performance of the inlet by adding a prepositive synergistic bulge in front of the anterior lip of the inlet is proposed in this paper. The performance of the baseline inlet and the synergistic bulge inlet is calculated and compared using a numerical calculation method. In addition, the mechanism of this synergistic bulge inlet configuration and the influence of design parameters are analyzed. The calculation results show:

1. The synergistic bulge diverts part of the low-energy boundary layer away from the inlet's entrance, which improves the inlet flow quality of the submerged inlet. There is a large velocity increase at the wall near the anterior lip in the inlet channel, which eliminates the separation vortex formed by low-energy fluid in the baseline inlet, and improves the performance of the submerged inlet. After setting the bulge, the total pressure recovery coefficient of inlet increased by up to 1.36%, total pressure distortion index decreased by 10.86%, and the projectile drag increased by 0.37%, which means the bulge can meet the design requirements.
2. The efficiency enhancement effect of the prepositive synergistic bulge inlet configuration is relatively stable. Among the three design parameters, the aspect ratio of bulge has the greatest influence on the aerodynamic performance of the inlet. When the aspect ratio is too small, not only the low-energy boundary layer at the inlet cannot be excluded, but also a low-pressure area will be formed after the synergistic bulge, which seriously reduces the inlet's performance. Therefore, it should be ensured that the aspect ratio is no less than 0.75. The additional drag brought to the projectile by the bulge increases with its height, and the drag increases by 0.86% compared with the baseline model when the bulge height is 5 mm.
3. Under different exit Mach numbers, incoming Mach numbers, attack angles, and sideslip angles, the method of adding the synergistic bulge before the submerged inlet can improve the performance of the baseline inlet, and the increment of the additional drag can basically meet the design requirements, meaning it has wide applicability. When the inlet exit's Mach number in the calculation condition is smaller or the incoming flow's Mach number is larger, the effect of this method on the improvement of the inlet's performance is more obvious.

Author Contributions: Conceptualization, B.M.; methodology, X.B.; data curation, X.B.; writing—original draft, X.B.; writing—review and editing, B.M.; supervision, B.M.; project administration, B.M. All authors have read and agreed to the published version of the manuscript.

Funding: This research was funded by the Fundamental research projects in characteristic disciplines, Grant No. G2023WD0124 and the National Natural Science Foundation of China, Grant No. 12202363.

Data Availability Statement: The relevant information of numerical calculation has been reflected in the manuscript in the form of pictures, charts, etc.

Conflicts of Interest: The authors declare no conflict of interest.

Nomenclature

d	Outlet diameter of the inlet
σ	Total pressure recovery coefficient
DI	Total pressure distortion index
P_m	Flow-weighted average total pressure on the exit of the inlet
P_∞	Total pressure of the incoming flow
$P_{AIP,\max}$	Maximum total pressure on the exit of the inlet
$P_{AIP,\min}$	Minimum total pressure on the exit of the inlet
P_{FAV}	Average total pressure on the exit of the inlet
M_0	Incoming flow Mach number
M_e	Inlet exit Mach number
α	Attack angle
β	Sideslip angle
D_0	Drag around the projectile with the baseline configuration
D_b	Drag around the projectile and the bulge with the synergistic bulge inlet configuration
$P_{AIP,0}$	Baseline inlet exit's flow-weighted average total pressure
$P_{AIP,b}$	Synergistic bulge inlet exit's flow-weighted average total pressure
L_x	Length of the bulge
L_y	Width of the bulge
L_{lip}	Width of the inlet's anterior lip
Δz	Height of the bulge
(x_0, y_0, z_0)	Coordinates of the initial point on the bulge
(x_b, y_b, z_b)	Coordinates of any point on the bulge
α_s	Swirl angle
U_θ	Circumferential velocity component at a certain point on the inlet's exit
U_x	Axial velocity component at a certain point on the inlet's exit

References

1. Jia, G.W.; Yin, P.; Shao, S.; Wang, J. Review of RCS measurement and imaging methods of stealth aircraft. *J. Natl. Univ. Def. Technol.* **2022**, *44*, 93–103.
2. Anderson, B.H.; Reddy, D.R.; Kapoor, K. Study on computing separating flows within a diffusion inlet S-duct. *J. Propuls. Power* **1994**, *10*, 661. [CrossRef]
3. Harloff, G.J.; Smith, C.F.; Bruns, J.E.; DeBonis, J.R. Navier-Stokes analysis of three-dimensional S-ducts. *J. Aircr.* **1993**, *30*, 526–533. [CrossRef]
4. Axelson, J.A.; Taylor, R.A. *Preliminary Investigation of the Transonic Characteristics of an NACA Submerged Inlet*; Technical Report Archive & Image Library: Washington, DC, USA, 1950.
5. Sun, S.; Guo, R.W. Numerical Analysis and Experimental Validation of a Submerged Inlet on the Plane Surface. *Chin. J. Aeronaut.* **2005**, *18*, 199–205. [CrossRef]
6. Sun, S.; Guo, R.W.; Wu, Y.Z. Characterization and Performance Enhancement of Submerged Inlet with Flush-Mounted Planar Side Entrance. *J. Propuls. Power* **2007**, *23*, 987–995. [CrossRef]
7. Wang, Y.G.; Wang, C.H.; Xiao, Y.C.; Chen, B.; Zhou, S.; Guo, J.T.; Sun, M.W. Construction methodology for lip surface of a submerged inlet. *Aerosp. Sci. Technol.* **2016**, *54*, 340–352. [CrossRef]
8. Mehdi, M.; Sajad, G.; Davood, T. Numerical Investigation of Geometrical Design Effect on the Submerged Inlet Aerodynamics Characteristics. *Int. J. Aeronaut. Space Sci.* **2020**, *21*, 25–38. [CrossRef]
9. Pei, H.; Cui, Y.; Kong, B.; Jiang, Y.; Shi, H. Structural parameters optimization of submerged inlet using least squares support vector machines and improved genetic algorithm-particle swarm optimization approach. *Eng. Appl. Comput. Fluid Mech.* **2021**, *1*, 503–511. [CrossRef]
10. Harper, D.K.; Leitch, T.A.; Ng, W.F.; Guillot, S.G. Boundary Layer Control and Wall-Pressure Fluctuation in a Serpentine Inlet. In Proceedings of the 36th AIAA/ASME/SAE/ASEE Joint Propulsion Conference and Exhibit, Las Vegas, NV, USA, 24–28 July 2000.
11. Owens, L.R.; Allan, B.G.; Gorton, S.A. Boundary-Layer-Ingesting Inlet Flow Control. In Proceedings of the 44th AIAA Aerospace Sciences Meeting and Exhibit, Reno, Nevada, 9–12 January 2006.
12. Ng, Y.T.; Luo, S.C.; Lim, T.T.; Ho, Q.W. Three Techniques to Control Flow Separation in an S-Shaped Duct. *AIAA J.* **2011**, *49*, 1825–1832. [CrossRef]

13. Harouni, A.G. Flow control of a boundary layer ingesting serpentine diffuser via blowing and suction. *Aerosp. Sci. Technol.* **2014**, *39*, 472–480. [CrossRef]
14. Keerthi, M.C.; Kushari, A. Effectiveness of vortex generator jets and wall suction on separated flows in serpentine-duct diffuser. *Aerosp. Sci. Technol.* **2014**, *34*, 12–19. [CrossRef]
15. Paul, A.R.; Joshi, S.; Jindal, A.; Maurya, S.P.; Jain, A. Experimental Studies of Active and Passive Flow Control Techniques Applied in a Twin Air-Intake. *Sci. World J.* **2013**, *2013*, 523759. [CrossRef] [PubMed]
16. Yadav, K.R.; Paul, A.R.; Hegde, N.; Jain, A. A Comparison of Circular and Slotted Synthetic Jets for Flow Control in a Twin Air-Intake. *Def. Sci. J.* **2020**, *70*, 113–121. [CrossRef]
17. Taskinoglu, E.S.; Knight, D.D. Design Optimization for Submerged Inlets—Part I. In Proceedings of the 41st Aerospace Sciences Meeting and Exhibit, Reno, Nevada, 6–9 January 2003; AIAA Paper 2003-1247.
18. Taskinoglu, E.S.; Jovanovic, V.; Knight, D.D. Design Optimization for Submerged Inlets- Part II. In Proceedings of the 21st AIAA Applied Aerodynamics Conference, Orlando, FL, USA, 23–26 June 2003; AIAA Paper 2003-3926.
19. Taskinoglu, E.S.; Jovanovic, V.; Knight, D.D. Multi-objective design optimization and experimental measurement for a submerged inlet. In Proceedings of the 42nd AIAA Aerospace Sciences Meeting and Exhibit, Reno, NV, USA, 5–8 January 2004; AIAA Paper 4478-4491.
20. Jovanovic, V.; Taskinoglu, E.S.; Knight, D.D. Experimental investigation of a submerged subsonic inlet. *Appl. Aerodyn. Conf. Exhib.* **2004**, *22*, 214–217. [CrossRef]
21. Pérez, C.C.; Ferreira, S.B.; da Silva, L.F.F.; de Jesus, A.B.; Oliveira, G.L. Computational Study of Submerged Air Inlet Performance Improvement Using Vortex Generators. *J. Aircr.* **2007**, *44*, 1574–1587. [CrossRef]
22. Cheng, D.S.; Tan, H.J.; Sun, S.; Tong, Y. Computational Study of a High-Performance Submerged Inlet with Bleeding Vortex. *J. Aircr.* **2012**, *49*, 852–860. [CrossRef]
23. Sun, S.; Tan, H.J.; Wang, C.X. Submerged inlet performance enhancement using a unique bump-shaped vortex generator. *J. Propuls. Power* **2016**, *32*, 1275–1280. [CrossRef]
24. Saheby, E.B.; Shen, X.; Huang, G.; Hays, A.P. Flow structure of the ridge integrated submerged inlet. *Aerosp. Sci. Technol.* **2021**, *119*, 107136. [CrossRef]
25. Xie, W.; Yang, S.; Zeng, C.; Liao, K.; Ding, R.; Zhang, L.; Guo, S. Effects of forebody boundary layer on the performance of a submerged inlet. *Aeronaut. J.* **2021**, *125*, 1260–1281. [CrossRef]
26. Xie, W.Z.; Zeng, C.; Wang, Z.Y.; Guo, S. Flow Control for a Submerged Inlet. *J. Fluids Eng.* **2022**, *144*, 121202. [CrossRef]
27. Askari, R.; Soltani, M.R. Numerical Simulation of a Y-Shaped Diverterless Supersonic Inlet. *J. Aircr.* **2023**. [CrossRef]
28. Tanguy, G.; MacManus, D.G.; Garnier, E.; Martin, P.G. Characteristics of unsteady total pressure distortion for a complex aero-engine intake duct. *Aerosp. Sci. Technol.* **2018**, *78*, 297–311. [CrossRef]
29. Gil-Prieto, D.; Zachos, P.K.; MacManus, D.G.; McLelland, G. Unsteady characteristics of S-duct intake flow distortion. *Aerosp. Sci. Technol.* **2019**, *84*, 938–952. [CrossRef]
30. Tanguy, G.; MacManus, D.G.; Garnier, E. Numerical investigation of the unsteady distortion for an S-duct intake with mechanical vortex generators. *Int. J. Heat Fluid Flow* **2022**, *95*, 108975. [CrossRef]
31. Patel, V.C.; Rodi, W.; Scheuerer, G. Turbulence models for near-wall and low Reynolds number flows: A Review. *AIAA J.* **1985**, *23*, 1308–1319. [CrossRef]
32. SAE International. *A Methodology for Assessing Inlet Swirl Distortion: AR 5686*; SAE International: Warrendale, PA, USA, 2010.